Interactions and Structure of the Nuclear Pore Complex Revealed by Cryo-electron Microscopy

Christopher W. Akey*‡

*Department of Cell Biology, Stanford University School of Medicine, Stanford, California 94305; and ‡Structural Studies Division, Medical Research Council Laboratory of Molecular Biology, Cambridge CB2 2QH, England

Abstract. Nuclear pore complexes (NPCs) play a central role in mediating nucleocytoplasmic transport and exchange processes in eukaryotic cells. The arrangement and interactions of NPCs within amphibian nuclear envelopes have been studied using cryo-electron microscopy of unfixed and frozen hydrated specimens. The nuclear lamina in *Necturus* forms an orthogonal network with crossover distances which vary between 1,600 and 4,000 Å and which may be related to the basic filament repeat of lamins. Furthermore, the NPCs are attached randomly within the confines of the lamin network, presumably by their nucleoplasmic rings. Image analysis of edge-on and en face projections of detergent-extracted NPCs has been combined with data on the coaxial thin rings to provide a quantitative evaluation of the triple ring model of NPC architecture proposed previously (Unwin, P. N. T., and R. Milligan. 1982. *J. Cell Biol.* 93:63–75). Additional details of the complex have been visualized including an intimate association of the inner spoke domains as an inner spoke ring, extensive domains within the spokes and coaxial thin rings, and interestingly, a central channel-like feature. Membrane-associated NPCs and detergent-extracted NPCs both possess peripherally located radial arms resulting in an effective diameter of ~1,450–1,500 Å. In projection, the radial arms possess approximate mirror symmetry suggesting that they originate from both sides of the assembly. Moreover, membrane-associated NPCs are asymmetric at most radii and right-handed as viewed from the cytoplasm; detergent-extracted NPCs appear to be symmetric and have ~822 symmetry. Taken together, the data suggests that the framework of membrane-associated NPCs is perturbed from a symmetrical configuration, either during isolation of nuclei or by interactions with the lamina and the nuclear envelope in vivo. However, detergent extraction of nuclei appears to result in a more symmetrical alignment of components in apposing halves of the assembly.

THE nuclear pore complex (NPC)[1] is a supramolecular assembly which spans the double-membrane system of the nuclear envelope in eukaryotic cells. Nucleocytoplasmic movements of ions, small molecules, and macromolecules are presumably mediated by the NPC and microinjection experiments suggest an exclusion limit of ~90 Å for passive exchange (4, 10, 46, 47). Recent studies have shown that a permanent nuclear localization signal is present in some large proteins which are imported into the nucleus (7, 12, 33, 48; but also see references 11, 45 for recent reviews). Furthermore, initial rates of protein import into *Xenopus* oocyte nuclei have been shown to be both saturable and sensitive to competition, indicating that transport is a receptor-mediated process (29). Nucleocytoplasmic transport has also been observed in reconstituted nuclei and is temperature dependent (42), requires ATP (42, 43), and is inhibited by wheat germ agglutinin (19). In addition, Feldherr and co-workers (18) have shown that the import of large nucleoplasmin-coated gold particles occurs through a centrally located region of the pore complex; thereby demonstrating that transport need not involve an unfolding of macromolecules smaller than ~260 Å in diameter. Ribosomal precursors and RNPs containing mRNAs and tRNAs are also exported from the nucleus by way of the NPC (15, 39, 53, 60) and the export of tRNAs has been characterized as a carrier-mediated translocation process (61).

The number of polypeptides which comprise the NPC is not known; however, a major glycoprotein of the NPC–lamina fraction, gp-190, has been localized to the periphery of the pore complex by immuno-electron microscopy and postulated to act as a membrane anchor (28). The carbohydrate moiety of gp-190 is presumably located in the cisternal space between nuclear leaflets as demonstrated by preferential binding of FITC–Con A to broken nuclei (19, 59). Recently, a second major class of eight novel glycoproteins which contain O-linked *N*-acetyl glucosamines and bind the transport

Christopher W. Akey's present address is Department of Biophysics, Housman Medical Research Center, Boston University School of Medicine, Boston, MA 02118-2394.

1. *Abbreviations used in this paper*: CTF, contrast transfer function; NPC, nuclear pore complex.

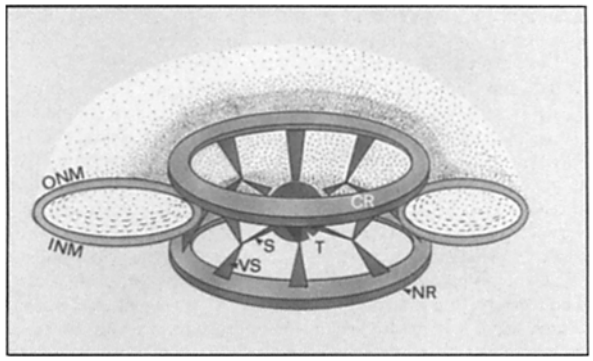

Figure 1. A three-dimensional ribbon model of the NPC excluding attachments to the lamina and nuclear envelope is shown. In close packed arrays, the nuclear envelope forms a hollow torus which is wrapped around the NPC like an inner tube on a rim. However, in actuality the torus is highly branched with four to six tubular arms radiating off to wrap around adjacent NPCs. The labeled components are the inner and outer nuclear membranes (*INM* and *ONM*), cytoplasmic and nucleoplasmic rings (*CR* and *NR*), spokes (*S*), vertical supports (*VS*), and the transporter assembly (*T*) (previously identified as the central plug or granule).

inhibitor wheat germ agglutinin (19), have been localized to the NPC (3, 8, 9, 52).

Initial models of NPC architecture have suggested a tripartite organization consisting of two annuli of discrete subunits (as opposed to rings) framing a central ring of subunits in which a central granule is sometimes present (22, 37, 49). Improvements in specimen preparation (17, 58) and the use of image processing (40, 58) have allowed a more complete description of the dominant structural features of the NPC. Electron microscopy of detergent-extracted nuclei and annulate lamellae has demonstrated that the NPC is built from supramolecular components including two coaxial rings located at the inner and outer surfaces of the nuclear envelope, a radially aligned central spoke assembly, and possibly a central plug (58). The major components of detergent-extracted NPCs were postulated to be symmetrically disposed about the center of the assembly in a manner consistent with 822 point-group symmetry (58), in agreement with subsequent single particle averaging of ~30 pore complexes (40). A ribbon diagram summarizing the triple ring model of the NPC proposed by Unwin and Milligan (58, 40) is presented in Fig. 1. The central spokes and the coaxial rings have been reduced in size for clarity. Furthermore, large particles tentatively identified as ribosomes (or ribosomal precursors) may be associated with the cytoplasmic surface of NPCs in some cases (22, 49, 58).

In this report, details are presented of the arrangement and interactions of NPCs with the lamina of amphibian nuclear envelopes, as visualized in frozen aqueous solution. Quantitative image processing of detergent-extracted NPCs has allowed verification of the triple ring model of NPC architecture proposed by Unwin and Milligan (58) and new details which pertain to the function of the NPC are described.

Materials and Methods

General

Female amphibians were obtained from Nasco Biologicals (Fort Atkinson, WI). *Xenopus laevis* were maintained in tanks an ambient room temperature; *Necturus maculosus* were kept at 4°C under minimal light conditions during the egg-bearing season and fed feeder goldfish every 7–10 d. Mature oocytes were surgically removed from either species after sedation by immersion in tricaine solutions (0.5 and 0.3 g/liter, respectively) for ~20 min. Oocytes were dissected from ovary clusters, rinsed, and stored on ice in Barths saline (30) with 0.2 mM $MgCl_2$, for 1–6 h before use.

Specimen Preparation and Cryo-electron Microscopy

Nuclei were isolated by extrusion under gentle pressure through holes formed in the animal hemisphere of the oocytes with a blunt needle. Adhering granular cytoplasm was then removed by gentle back and forth pipetting within a 100-μl silanized microcapillary. In some instances, the nuclei were detergent extracted with 0.1% Triton X-100 as described (58). The nuclei or nuclear ghosts were subsequently transferred in low salt buffers onto appropriate support grids which were previously glow discharged in amyl amine (13). The nuclei were then gently splayed open with fine glass needles and allowed to become firmly adhered to the grids; the nucleoplasm was then removed. Cryo-specimens were prepared by blotting followed by rapid freezing in liquid nitrogen-cooled ethane slush and were subsequently stored in liquid nitrogen (14). Samples were loaded into a Gatan, Inc. cryostage (model 626 mark I; Warrendale, PA) under liquid nitrogen and transferred to a Philips Electronic Instruments, Inc. electron microscope (model 400T; Mahwah, NJ) equipped with an additional two-bladed anticontaminator (32). After sublimation of the solid ethane layer, the specimens were cooled to −177°C and minimal dose images (one to two electrons per angstrom squared) were recorded from areas in amorphous ice with the low dose kit. Micrograph pairs were taken at magnifications of 10,000–13,000 at 80 kV with a 50-μm objective aperture and nominal defocus values of 6.4 and 19.2 μm. The position of the first zero of the contrast transfer function in the initial micrograph used for processing occurred at a spacing of ~1/50 reciprocal angstroms. Magnifications were obtained by calibrating the specimens z-height, as a function of in-focus objective lens current using a replica line grating (Pelco, Inc., Tustin, CA; 21,600 cm/line). Subsequently, the in-focus current was recorded from an external meter (designed by C. Toyoshima, Stanford University School of Medicine, Stanford, CA) for all micrographs and used to calculate a z-height adjusted magnification.

Image Processing

Micrograph selection criteria included the usual constraints on astigmatism and drift; initial images were processed if a large proportion of the NPCs were circular and demonstrated eightfold symmetry in the second more highly defocused image. As observed previously for large structures, only specimens totally embedded in amorphous ice were well preserved (41). Additional constraints on the calculation of averages were imposed by sample heterogeneity and distortions; therefore, only 15–40% of the NPCs were taken for processing from the best images and a single projection map (in all 25 separate averages were determined) was always obtained from a series of micrographs from adjacent areas of the same specimen grid (usually the same grid hole). This insured that local conditions at the time of freezing were comparable for all the NPCs in a given average. Complete micrographs were densitometered on a Perkin-Elmer Corp. microdensitometer (Norwalk, CT) 1010A, at a sample step and aperture size of 25 μm in blocks of roughly 1,500 × 1,500 pixels. Particles for analysis were chosen from images displayed on an AED-512 or -1024 with a program written to do displays and interactive particle selection from a single particle image processing program (SPIDER)-formatted files, outside of the SPIDER driver (21). Appropriately windowed and masked particles (routinely 100–350 at a time) were rotationally aligned by angular cross-correlation in real space and centered by cross-correlation against a reference obtained from an eightfold average of an initial refinement of ~100 particles. In addition, alignments were also done in which the initial references were not eightfold averaged. The resulting maps were essentially identical to those from averages which were calculated with enforced references. Alignment parameters for the datasets usually converged in two to three iterations. Refined projection maps were eightfold averaged and maps resulting from 20–30 NPCs demonstrated a visual convergence of major structural features when compared with the final 200–300 particle datasets. The final database contains ~5,000 aligned pore complexes. The resolution of the projection maps is typically ~65–70 Å as determined by Fourier ring correlation in SPIDER and appears to be limited by an inherent flexibility of the complex coupled with a variability of the center channel region. A summary of the datasets is given in Table I. Some heterogeneity was observed in averages of membrane-

Table I. Summary of NPC Projection Datasets

Type	Form*	Structures	NPCs	Redundancy§	Films
Necturus	D	3	410	3,280	9
Necturus	M	2	504	4,032	8
Xenopus	M	3	655	5,240	9
All‡	M and D	25	5,029	40,232	53

* *D*, detergent-extracted form; *M*, membrane-associated form.
‡ Data for the entire database (excluding the rings and edge-on views) are presented in this category.
§ Total number of rotationally equivalent units in point group 8.

associated NPCs from *Necturus* which appeared to be correlated with the osmotic conditions at the time of freezing. However, the major features in maps of membrane-associated NPCs presented herein are representative of all the datasets.

Effect of the Contrast Transfer Function (CTF)

In this study, projection maps of NPCs were obtained from micrographs of defocused specimens (6.4 μm); hence the predominant source of image contrast in these images should be phase contrast (16, 57). The effect of the CTF on the interpretability of image features in the resulting averaged maps was evaluated. Paired micrographs of detergent-extracted NPCs were recorded at 10- and 22-μm defocus and processed in parallel. After alignment and correction of the images for a 2.5% change in magnification, the amplitude ratios from the molecular transforms in the resolution range of 1/400–1/90 Å were compared as a function of defocus and the contribution of amplitude contrast was evaluated essentially as described by Toyoshima and Unwin (57). The data indicated a contribution of 6–10% amplitude contrast in agreement with values determined at higher resolution (57). As a test, images were subsequently corrected a number of ways including: (*a*) using 7% amplitude contrast; (*b*) using 20% amplitude contrast; and (*c*) by adding images taken at the two rather different defocuses after low pass filtering to their first zero in the CTF. After correction, the relative strengths of image features were altered (as expected) and the radial positions of most peaks in the maps were unchanged except near the particle centers. This latter effect is due to the truncation of higher resolution components in the more highly defocused image which affect the position of these near axis peaks. Modulation of the true image transform by the CTF acts to boost the high resolution components in the image. In general, the shapes of features were similar though their boundaries were less sharp. The micrographs used in this study were chosen for their preservation of a central channel feature in the NPCs and this feature was present in reconstructions from both the 10- and 22-μm defocused images. Features very near the center of the maps should be correct as long as a proper defocus is used in recording the micrograph, such that all image frequencies in the resulting average above the background level are transmitted with the proper relative phase. All the images processed in this work fulfilled this criteria. In as much as the original projection maps are reasonably accurate representations of the projected density, these maps are presented in this work without modification.

Results

In this report I will first present data on the arrangement of NPCs and the lamin network in *Necturus* nuclear envelopes. Subsequently, data will be presented which allows a quantitative evaluation of the triple ring model of NPC architecture (58). Finally, projection maps of both detergent-extracted and membrane-associated NPCs will be compared and a revised architectural model is presented in the Discussion.

Arrangement of the Nuclear Envelope

The amphibian oocyte provides a remarkable system to study the structure and function of the nuclear envelope and its ma-

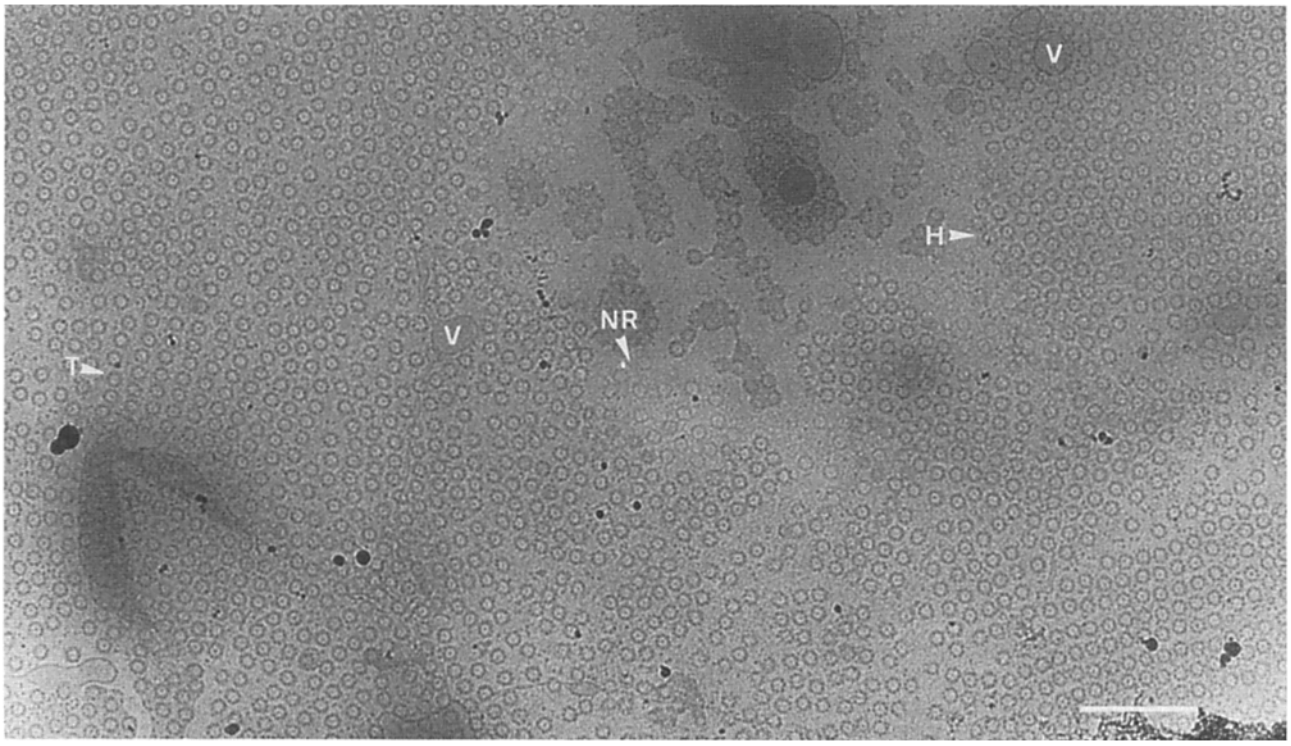

Figure 2. A low magnification image of a spread nuclear envelope from *Necturus* is shown in amorphous ice. The NPCs are packed in square arrays in many areas, as the result of their interactions with the underlying lamina. Some areas have undergone demembranation due to osmotic swelling (*V*, vesicles). In areas of membrane loss some nucleoplasmic rings are retained (*NR*). The NPCs are often packed in tetragonal and hexagonal arrays (*T* and *H*). Some membrane-associated particles are also present between the NPCs and may correspond to ribosomes. Bar, 10,000 Å.

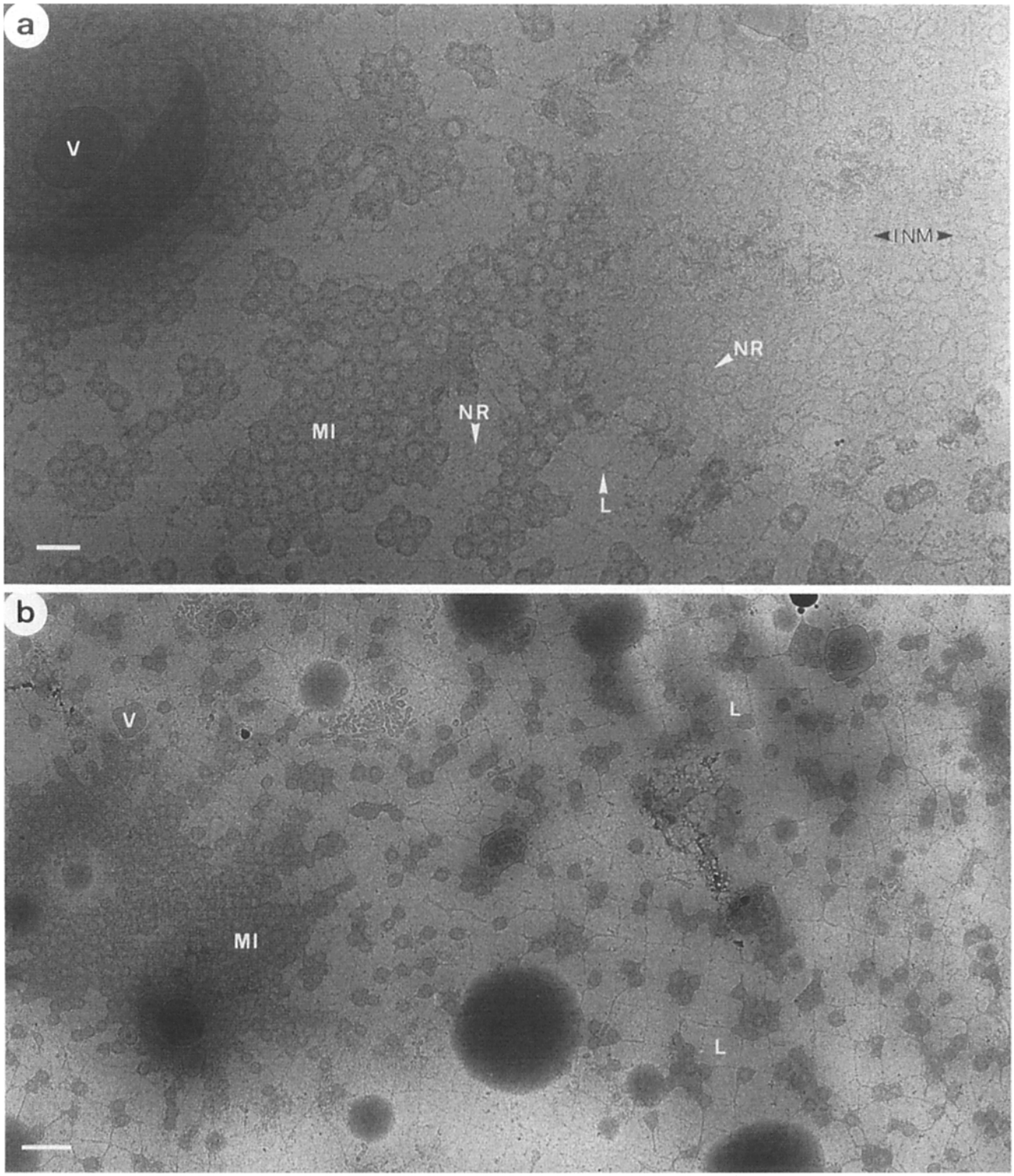

Figure 3. (*a*) An area of osmotically shocked nuclear envelope caught in various stages of disassembly. NPCs in membrane islands are well preserved in amorphous ice (*MI*). In some regions the cytoplasmic rings and spoke assemblies have been lost leaving behind the nucleoplasmic rings (*NR*), the inner nuclear membrane (*INM*), and the lamina (*L*). (*b*) An area of osmotically shocked nuclear envelope from *Necturus* is shown in which the lamina is orthogonally arrayed with a crossover repeat of ~3,000–4,000 Å. Note that the NPCs left associated with the lamina are still packed in their own islands of nuclear envelope. Bars: (*a*) 2,500 Å; (*b*) 5,000 Å.

jor constituents, the NPC and the underlying lamina. The NPC packing density in spreads of nuclear envelopes from *Xenopus* and *Necturus* may approach 30–45 NPCs/μm^2 representing the density achieved in square arrays (*Necturus*) and hexagonal packing (*Xenopus*). A typical highly ordered area of nuclear envelope from a *Necturus* oocyte, in amor-

phous ice, is presented in Fig. 2. The NPCs tend to align locally in rows and tetragonal arrays (Fig. 2, *T*) with less regular areas interspersed. Based on observations of ~500 nuclei, the global arrangement of NPC domains in *Necturus* nuclei consists of large dense-packed continents of NPCs surrounded by membrane areas of lower NPC density and less regular packing. In some instances the dense-packed areas may be hexagonally packed (Fig. 2, *H*) rather than square packed. The reasons for this large scale segregation phenomenon are not known, but may reflect lamina organization and, to some extent, the deformation resulting from osmotic swelling during isolation. The amphibian nucleus is sensitive to osmotic shock: during preparation some areas undergo vesicularization and demembranation with the concomitant loss of NPCs (Fig. 2, *V*), leaving behind the lamina meshwork and in some cases the attached nucleoplasmic coaxial rings from the NPC (see Fig. 2, *NR*, and model in Fig. 1).

NPC–Lamina Interactions

The nuclear lamina in *Xenopus* oocytes can form a network of orthogonally arrayed filaments with an average crossover spacing of 520 Å (2) and is composed primarily of lamin III (35). The lamina is thought to possess attachment sites for the inner nuclear membrane (22, 24) and chromatin (36). The lamina is masked in images of intact nuclear envelopes embedded in amorphous ice (for example see Fig. 9); however, the underlying lamina becomes visible after demembranation using either osmotic shock (see Fig. 3, *a* and *b*) or detergents (Fig. 4, *a* and *b*). The NPC is attached to the nuclear lamina (1, 2, 54) and images of osmotically shocked nuclei often demonstrate regions where the cytoplasmic coaxial rings and spoke assemblies have been lost, leaving the nucleoplasmic coaxial rings attached to the lamina and, in some instances, a sheet of the inner nuclear membrane (see Fig. 3 *a*).

A low magnification image of a *Necturus* nuclear envelope which has been Triton X-100 extracted and embedded in amorphous ice is shown in Fig. 4 *a*. The lamina forms an array of filaments as indicated by the series of arrows in Fig. 4 *b* (view the figures at a glancing angle). The lamin network has crossover spacings of between 1,600 and 2,000 Å and the NPCs are localized randomly between the lamina strands. Finally, the arrangement of ordered NPC–lamina domains forms a mosiac pattern. A second type of lamina packing observed in spread nuclei is shown in Fig. 3 *b*. In these areas, the average crossover spacings vary widely with a mean of 3,000–4,000 Å. The larger arrays do not appear to simply result from specimen deformations; the arrays are uniform and associated islands of NPCs and membranes show no indication of having been stretched.

A regular alignment of the lamina was previously demonstrated in *Xenopus* oocyte nuclei and proposed for rat liver nuclei (2). The existence of related lamina arrays in *Necturus* oocyte nuclei confirms the observation in *Xenopus*; however, a general packing model for the lamina with a defined crossover spacing awaits further investigation. Conceivably, a small family of lattice nets with crossover distances related to the 520-Å repeat of the lamins may exist (2, 20). The lattices in *Necturus* are roughly three- to eightfold larger than in *Xenopus*. Furthermore, ordered arrays of NPCs have been reported in freeze-etched root tip nuclei from *Selaginella kraussima* (55) with average spacings of 2,800 Å in either square or hexagonal arrays. The observed distances are too great for NPC–NPC interactions, but may represent a specific arrangement of NPCs on an ordered lamina. In general, the observation of ordered NPCs with lattice constants greater than ~1,500 Å may suggest a periodic underlying lamina; however, the low surface density of NPCs in most eukaryotic nuclei (37) may preclude the formation of ordered NPC arrays.

Edge-on Views and Rings

The structure of the NPC has been studied over a period of ~20 yr and architectural models have evolved as improvements in specimen preparation and computational analysis have been made. Elements of the early models of Franke (22) and Roberts and Northcote (49) have recently been incorporated into the triple ring model proposed by Unwin and Milligan (40, 58). This model is shown schematically in Fig. 1 and consists of a central ring of massive spokes (reduced in size for clarity), framed top and bottom by two thin coaxial rings. The data presented in the following two sections allows a quantitative evaluation of this model. In this work, the noncrystallographic image averaging methods developed by Frank (21) have been applied to micrographs of specimens preserved in frozen aqueous buffers (14). Initially, the projected structures of edge-on views of the intact NPC and isolated thin rings are described and this data is subsequently combined with averages of intact NPCs viewed along the eightfold axis.

Detergent extraction of nuclei results in nuclear ghosts comprised of lamina and attached NPCs (1). Occasionally, the NPCs flip over to give a trilamellate edge-on view and more rarely oblique views (see insets *1*, *2*, and *4* of Fig. 4 *b*). A projection map from 23 edge-on views is presented in Fig. 5 *a*. All maps in this work are presented as greyscale images with protein regions white. The eightfold symmetry axis of the NPC when viewed from the side (at 90°), degenerates into a twofold axis of symmetry for any view. The initial edge-on average also demonstrated well-defined twofold symmetry about the horizontal axis relating apposing halves of the assembly. Both symmetries have been incorporated in the map in Fig. 5 *a*. However, the resulting map is similar in all features to the original average. The dimensions of the NPC viewed edge-on are 1,200 × 730 Å. The central thick band of density corresponds to the spoke assembly as seen in thin sections (49). Furthermore, the trilamellate motif has been observed previously in negatively stained preparations of detergent-extracted NPCs (40, 58) and tilting experiments indicated that the central band of density behaves as expected for a ring of spokes. The two outer bands presumably correspond to the cytoplasmic and nucleoplasmic coaxial rings as observed in oblique views (see inset *4*, Fig. 4 *b*; also references 40, 58). In support of this assignment, the density modulation observed in the outer bands closely mimics that expected for a ring of subunits whose long axes are aligned circumferentially and viewed edge-on (see below). A further confirmation of the triple ring architecture of the NPC is obtained from edge-on views of partially disassembled NPCs attached to the lamina. In well preserved areas of detergent-extracted NPCs, the edge-on views are

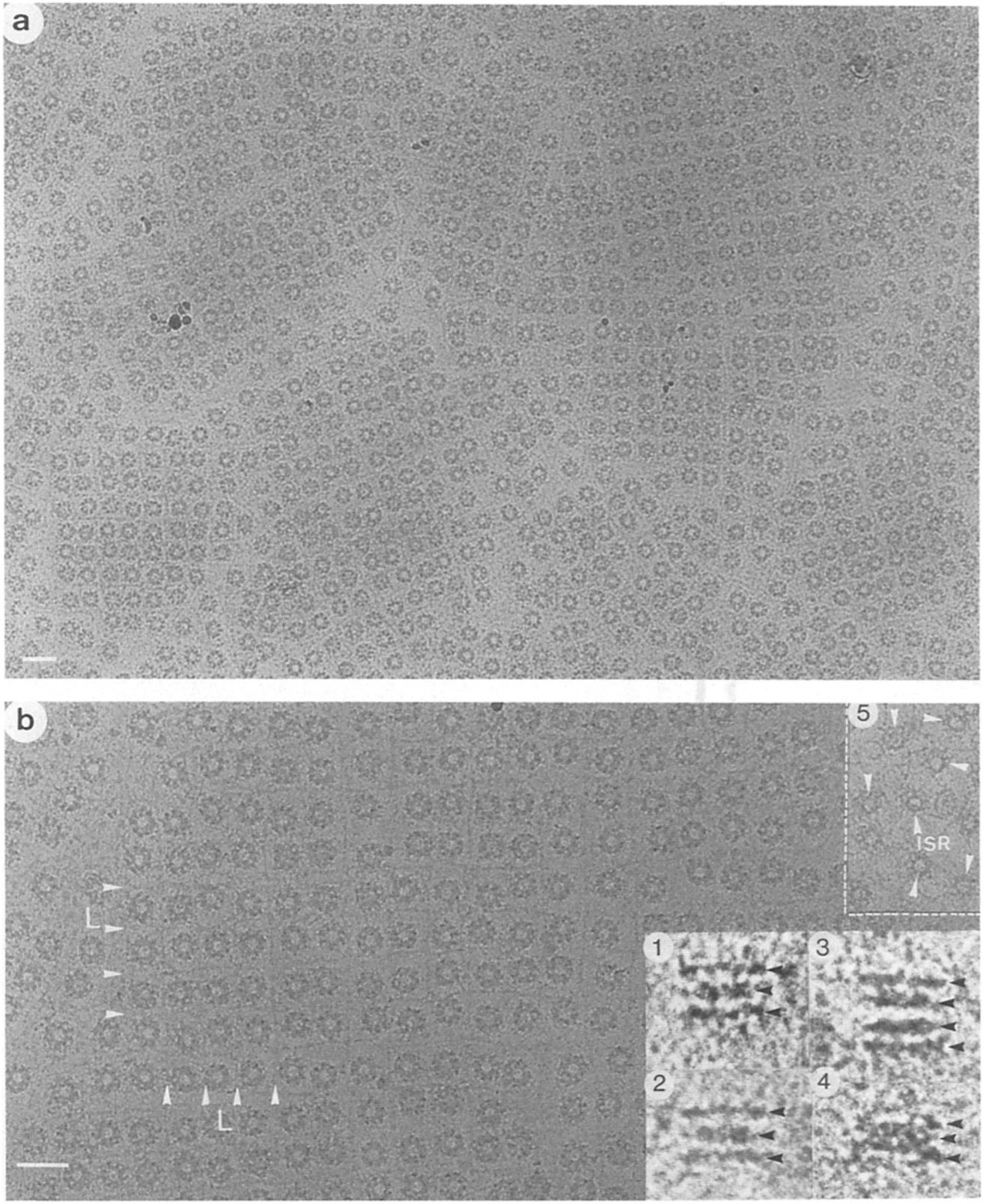

Figure 4. (*a*) A low magnification image of a detergent-stripped and spread nuclear envelope from *Necturus* is shown. The NPCs form arrays as the result of their interactions with the periodic lamina. (*b*) A higher magnification image of a portion of the field shown in *a*. The packing of the lamina strands is indicated by arrows, arrayed approximately at right angles. The overall appearance is like that of checkers on a checkerboard, with the NPCs packed between the lamina strands (average spacing is 1,900 ± 190 Å). (Insets *1* and *2*) Trilamellate edge-on views from an area of well preserved detergent-extracted NPCs. (Inset *3*) Bilamellate edge-on views of two adjacent NPCs in a poorly preserved area. (Inset *4*) An oblique view of a detergent-extracted NPC attached by its nucleoplasmic ring to the lamina. (Inset *5*) NPCs from a distorted area show that the inner spoke ring remains intact while the outer spokes and vertical supports are disordered, presumably as the result of their loss of the cytoplasmic coaxial rings. In insets *1–4* the length of the edge-on views is 1,200 Å. Inset *5* is the same scale as *b*. Bars, 2,500 Å.

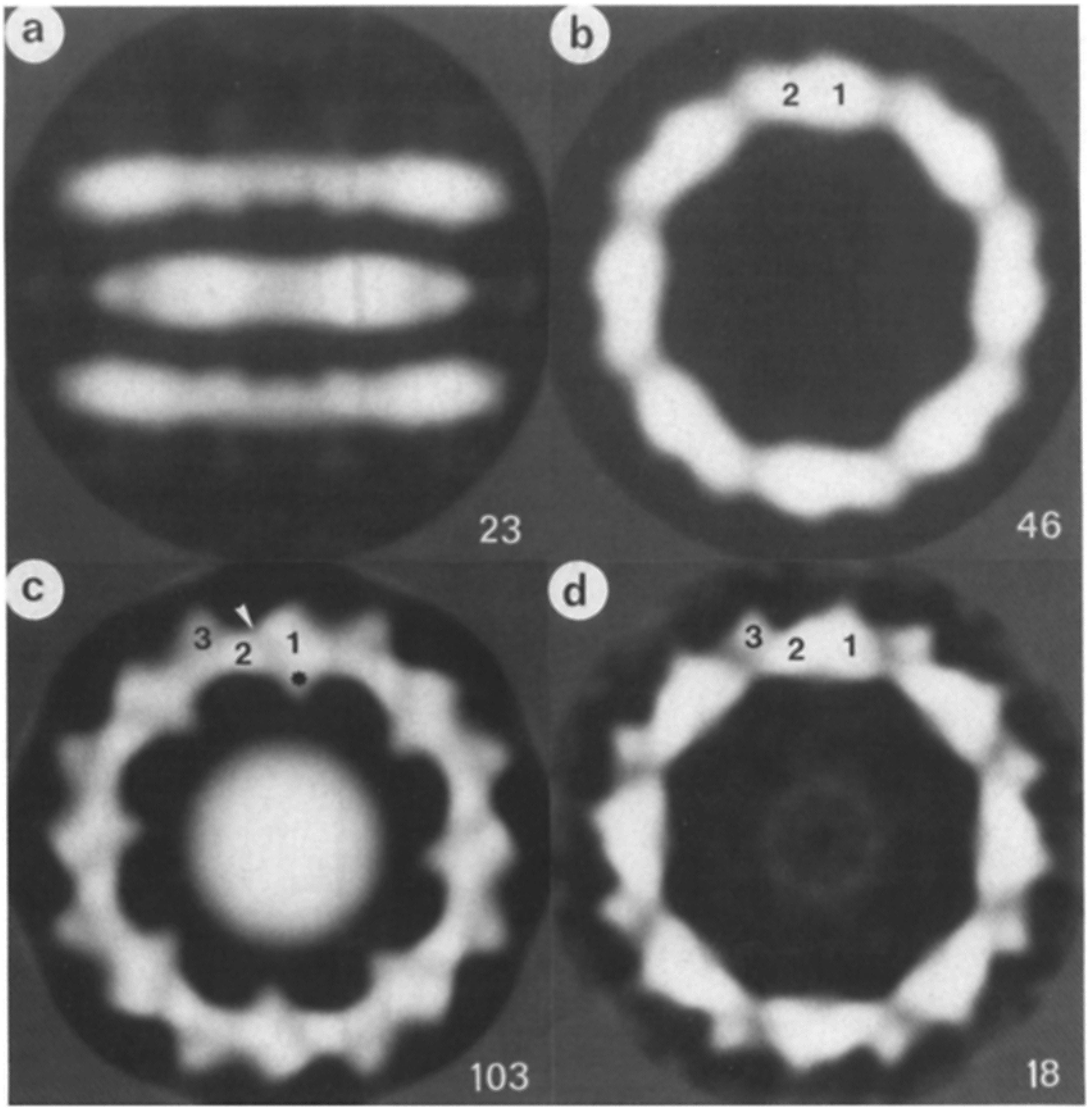

Figure 5. (*a*) Map of edge-on view from 23 NPCs. Protein is white. (*b*) Map of en face view of lamina-associated rings (n = 46). Two subunit domains are indicated. (*c*) Map of negatively stained cytoplasmic rings (n = 103). The rings are strongly modulated with four internal domains within the rotationally equivalent unit. The center density is an artifact of negative staining and does not represent protein structure. (*d*) Map of inner nuclear membrane-associated rings (n = 18). The ring subunit has three internal domains in equivalent positions to those observed in the negatively stained rings.

trilamellate; edge-on views in poorly preserved areas are usually bilamellate (see the two adjacent "half" NPCs in inset *3* of Fig. 4 *b*). The NPCs appear to preferentially lose their cytoplasmic coaxial rings and this may be correlated with the disordered appearance of the en face views.

Thin coaxial rings are sometimes observed in osmotically shocked nuclear envelopes which are undergoing disassembly. The rings appear to be attached to the lamina; hence, they may represent nucleoplasmic rings. As shown in Fig. 3 *a*, the rings are sometimes found in association with the lamina and a sheet of the inner nuclear membrane. Images of 46 lamina-associated rings and 18 membrane-associated rings were aligned and averaged separately and the projection maps are presented in Fig. 5, *b* and *d*. For comparison, a micrograph of negatively stained rings obtained by dissociating rings from the cytoplasmic face of the nuclear envelope was analyzed (58; micrograph provided by P. N. T. Unwin, Stanford University School of Medicine). The map from 103 cytoplasmic rings is presented in Fig. 5 *c*. The two ring averages from specimens in amorphous ice are qualitatively similar but also show significant differences. Both structures have approximately bilobed subunits with their long axis (~470 Å) aligned circumferentially. The outer edge of the ring in Fig. 5 *b* is smoother and the arrangement of the two domains differs from that in Fig. 5 *d*. Furthermore, the ring in Fig. 5 *b* is conspicuously missing the outer domain (marked *3*) in the map in Fig. 5 *d*. The reasons for the differences in the two maps are not understood, but maps of half datasets gave similar results. The projected structure of negatively stained cytoplasmic rings agrees well with the map in Fig. 5 *d*. Both have a jagged, external edge and their subunits have three similarly positioned domains (marked *1–3*). However, the cytoplasmic rings have a pronounced cleft of stain between domains *1* and *2* (see arrow) and an additional domain at the inner radii (see asterisk, Fig. 5 *c*). Conversely, the nucleoplasmic rings appear to have a more pronounced sub-

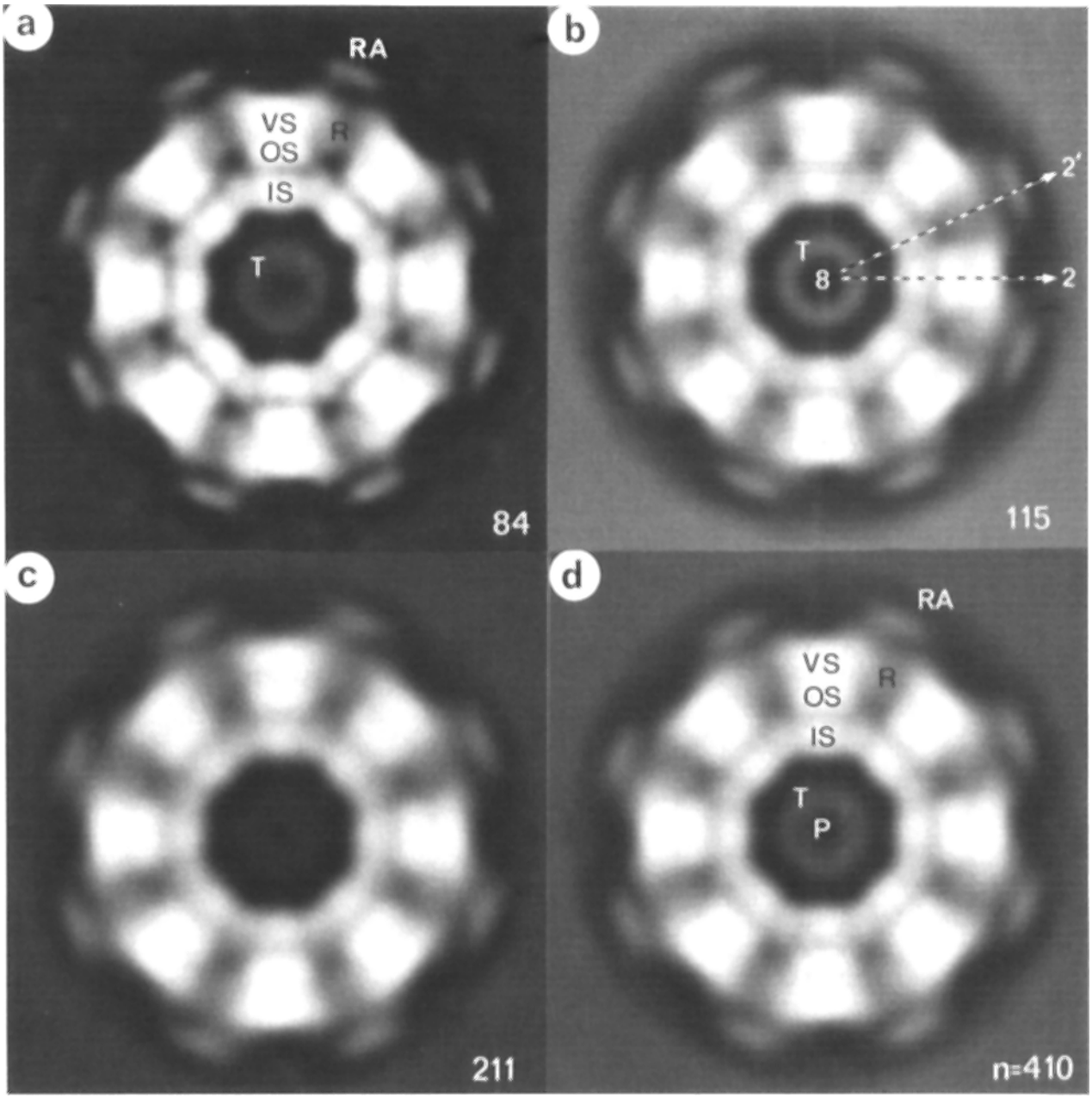

Figure 6. Individual and global averages of detergent-extracted NPCs are shown as projection maps. (*a*) A representative average from 84 particles (one structure) is presented. The contrast has been reversed and corresponds to that found on the original negatives, protein is white. Major structural features of the NPC include the inner spoke domain (*IS*), the outer spoke domain (*OS*), the vertical supports (*VS*), the coaxial rings viewed en face (*R*), and the radial arms (*RA*). In addition, a weakly contrasted central pore is visible. (*b*) Projected structure of 115 NPCs. Note the presence of a hollow central channel-like feature. The position of the twofold axes in a rotationally equivalent unit are indicated by dashed and arrowed lines. (*c*) A third projection of the detergent-extracted form (n = 211). (*d*) Average of three separate maps (n = 410). The weaker features in the maps are well preserved between the different structures. The various domains are labeled as in *a*. *T*, central transporter; *P*, central pore.

unit division circumferentially. A three-dimensional reconstruction of intact NPCs may resolve the question of whether the apposing rings have somewhat altered structures. However, the subunits of the nucleoplasmic rings may have undergone a progressive structural change during disassembly of the nuclear envelope before imaging. Finally, the observation of edge-on views of intact and half NPCs and of the nucleoplasmic and cytoplasmic rings, supports the triple ring model of NPC architecture proposed by Unwin and Milligan (58).

Detergent-extracted NPCs

Detergent-extracted NPCs (410 in three separate datasets) were subjected to alignment and single particle averaging (21) and the resulting maps are presented in Fig. 6. As

Table II. Spacings of NPC Components Viewed En Face or Edge-on

	Inner radius	Outer radius	Peak radius	Radial length	Maximum radial width	Maximum* in Z
	Å	Å	Å	Å	Å	Å
Transporter	0	160	–	–	–	–
Inner spokes	240	360	300	120	130	–
Outer spokes	360	470	430	85	170	–
Entire spokes	240	470	–	230	270	250
Vertical supports	490	600	540	110	–	–
Coaxial rings	400	600	–	200	470	100–130
Radial arms	600	720–760	–	~160	~80	–
Membrane border	–	–	360–470	–	–	–

* Vertical dimensions were obtained from edge-on views.

deduced previously (40, 58), detergent-extracted NPCs possess ~822 symmetry in projection. This implies that the packing of the major components within the NPC is determined by an axis of eightfold rotational symmetry aligned perpendicular to the nuclear envelope surface, coupled with an axis of twofold rotational symmetry which occurs between the inner and outer nuclear membranes and is perpendicular to the eightfold axis. In all there are two unique twofold axes repeated eight times round a circle for a total of 16. The arrangement of the twofold axes as viewed along the eightfold axis is shown in Fig. 6 *b*. The twofold axes when viewed from the side and in projection describe lines of mirror symmetry about which image features appear to be reflected. Mirror symmetry has not been imposed in Fig. 6; however, NPCs which demonstrated an obvious handedness were excluded from averaging as they appeared elliptically distorted or unraveled (see inset *5*, Fig. 4 *b*). The projection map of detergent-extracted NPCs is in good agreement with a previously reported map (40) determined from ~30 negatively stained NPCs from *Xenopus* (possibly from annulate lamellae as there was no adhering lamina in the specimens). The correspondence of the major features between the maps of specimens preserved in stain or amorphous ice was not unexpected (41).

New features termed the radial arms are visualized in these maps and project ~125 Å out past the border of the NPC proper (1,200 Å diameter), resulting in an effective total diameter of ~1,450 Å. The radial arms are nearly mirror symmetric as expected if the densities arose from the two sides of the NPC, rather than one face. A second new feature of the maps is the weak density located between the spokes at radii of 440–600 Å (Fig. 6, *a* and *d*, *R*). This density probably corresponds to the coaxial rings viewed en face; the density between the spokes is ~160 Å wide (see Fig. 5, *b–d*, and Table II). The precise alignment of the rings and their absolute hand relative to the spoke assembly is not known. However, based on the density and apparent width of the features between the spokes, the coaxial rings are probably aligned such that their elongated subunits overlay the spokes. This configuration places the intersubunit regions of the rings between the spokes. Additional features in the maps include three peaks within the radially aligned spoke assembly. The peaks occur at radii of 300, 430, and 540 Å and correspond to the inner spoke domains (Fig. 6, *IS*), the outer spoke domains (Fig. 6, *OS*), and the vertical supports of the thin rings (Fig. 6, *VS*) and are in agreement with values reported earlier (40). Based on maps of the edge-on view and the rings, the density at high radius (Fig. 6, *a* and *d*, *VS*) probably corresponds to a superposition of the subunits of the two apposed rings and the vertical supports observed in cross sections in the literature (49). The dimensions of relevant features in the maps in Figs. 5 and 6 are given in Table II.

As in previously determined maps, the spokes are bisected radially by an approximate line of mirror symmetry and the demarcation between the inner and outer spoke domains suggests a subunit division within the spokes radially (see Fig. 6 *d*). The eight inner spoke domains appear intimately associated in the detergent-extracted NPCs forming an inner spoke ring (see Fig. 6 and inset *5* of Fig. 4 *b*). Finally, few plugs or central granules were observed in images of unfixed detergent-extracted NPCs; instead, a low density (somewhat hollow) feature is centrally located in the region where transport of nucleoplasmin–gold is known to occur (18) and a montage of individual NPCs which show this feature is presented in Fig. 7.

The reproducibility of the weakest features in the maps (i.e., the radial arms) is demonstrated by a comparison of the three separate datasets (see Fig. 6, *a–c*) with the total average in Fig. 6 *d*. In addition, a central channel-like feature is present in many NPCs in micrographs (see Fig. 7). The strength of this feature in the maps is rather variable due to differences in preservation of the particle centers and to the possible presence of multiple structures. Furthermore, maps calculated with a 7% amplitude contrast correction still retained the radial arms and the channel-like feature with a central pore (see Materials and Methods; CTF).

The domain structure of detergent-extracted NPCs can also be visualized by plotting projected densities along the two unique twofold axes in the maps (see Fig. 6 *b*). Fig. 8 presents a density plot along the twofold axis (marked *2* in Fig. 6 *b*) as a solid curve. The three spoke domains are readily resolved (i.e., *IS*, *OS*, and *VS*/*R*) and the similarity of the curve about the particle center is another measure of the preservation of mirror symmetry about the twofold axes in the averaged map. In addition, the central pore and a weak smeared density corresponding to the NPC transporter (3) is observed (Fig. 6, *P* and *T*). The density plot along the twofold axis (labeled *2'* in Fig. 6 *b*) is presented as a dashed curve. The connecting density between the inner spoke domains (*IS*, Fig. 6) is clearly resolved as are the densities for the rings and the radial arms (Fig. 6, *R* and *RA*).

Overall, the structure of the detergent-extracted NPCs allows an insight into the three-dimensional architecture of the pore complex when combined with edge-on views and data

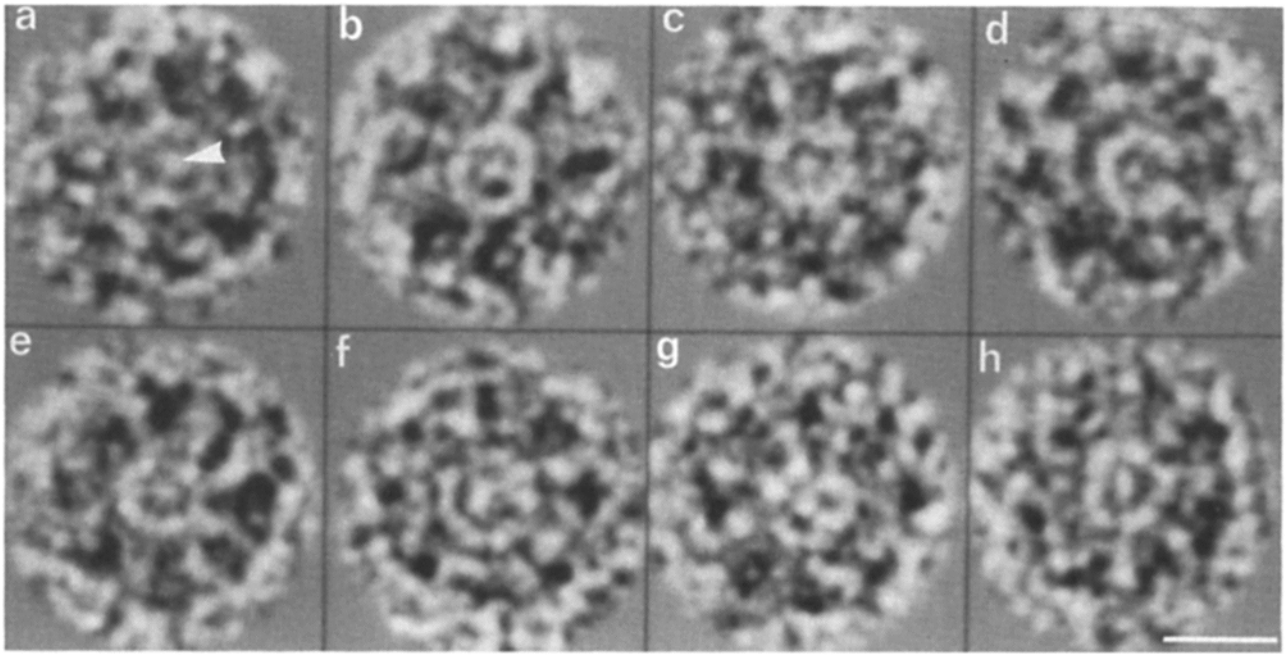

Figure 7. A montage of aligned detergent-extracted NPCs after low pass filtration which demonstrate a central channel-like feature (the NPC transporter; see reference 3). The protein is black as in original prints. Bar, 600 Å.

from the coaxial rings and this information is incorporated into the triple ring model of NPC architecture presented in the Discussion section.

Membrane-associated NPCs

Representative images are presented in Fig. 9 of nuclear envelopes from *Necturus* and *Xenopus* embedded in amorphous ice. In general, demembranated areas of the nuclear envelope revealed the lamina, whereas the lamina was difficult to observe in intact areas (compare Figs. 4 *a* and 9 *a*). A second criteria for the presence of the membrane was the appearance of a high density ring within the NPCs between radii of 360–470 Å attributable to the nuclear envelope (58). The membrane spaces between the NPCs appeared granular and as the thickness of amorphous ice decreased or the apparent salt concentration increased, the membranes became more transparent and the lamina could be observed weakly (view Fig. 9 *b* at a glancing angle). Occasional images also had large particles presumed to be ribosomes located in the spaces between the NPCs (see Fig. 9 *c*). In this study, direct evidence for an association of ribosomes with the cytoplasmic ring of the NPC was not obtained. However, the nuclei were unfixed and the specimen preparation conditions may not have been optimal for visualizing this association. Evidence for the triple ring model of the NPC was also obtained from fortuitous images of NPCs ejected from membrane folds and viewed obliquely (see inset, Fig. 9 *c*).

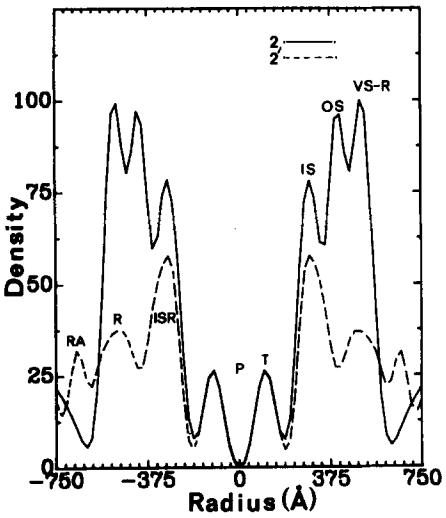

Figure 8. A plot of the projected density along the twofold axis labeled *2* in Fig. 6 *b* is shown as a solid curve. Note that the three major domains of the central spokes are delineated including the inner spoke domain (*IS*), the outer spoke domain (*OS*), and the vertical supports (*VS*). The central density from the global averages of the transporter and the central pore are also apparent (*T* and *P*). A plot along the twofold axes labeled *2'* in Fig. 6 *b* is shown as a dashed curve. Weaker features of the map are easily visible and include the inner spoke ring (*ISR*), the coaxial rings (*R*), and the radial arms (*RA*).

The structure of NPCs in isolated nuclei is intrinsically more variable than that of detergent-extracted NPCs. In some cases the periphery may be decorated with large particles (6, 31, 58) and a central granule or plug may be present (22, 40, 49, 58). Therefore, specimen areas used in processing were carefully chosen. Analyses of 22 separate averages representing ~4,600 membrane-associated NPCs, indicated that the region of greatest variability (besides the central channel) corresponded to the superposition of the coaxial rings and the vertical supports. Within a given structure from a single specimen area, the image features of the NPC were extremely reproducible. In fact, maps from 20–30 NPCs gave similar results for positions and shapes of the major structural features when compared to complete datasets of

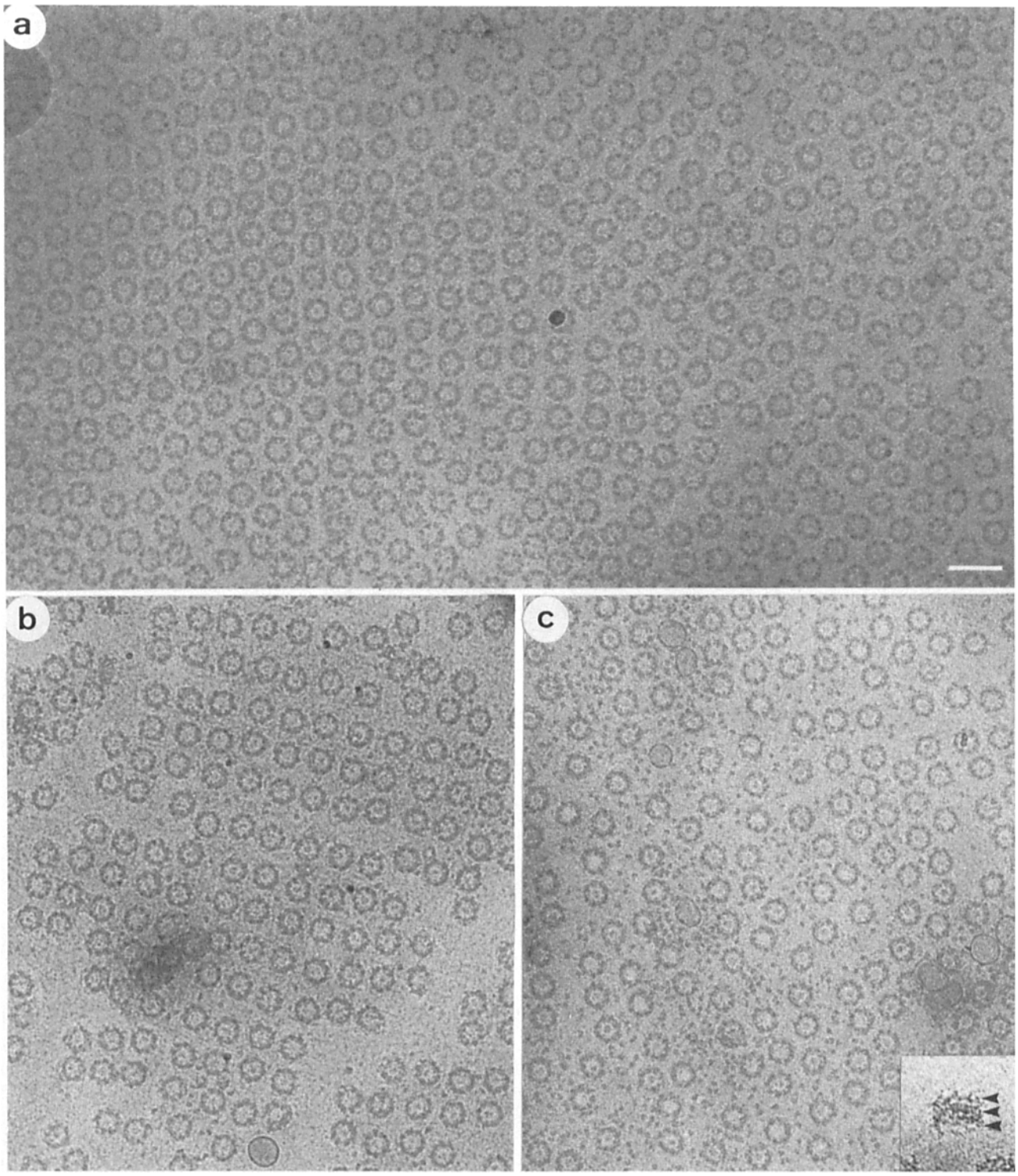

Figure 9. (*a*) An atypical image of membrane-associated NPCs from *Necturus* in amorphous ice is shown. The NPCs are square packed very tightly (average spacing is 1,530 ± 40 Å). Protein and strongly scattering matter is dark. (*b*) A second typical field of membrane-associated NPCs from *Necturus* is shown. Note the granularity of the membrane spaces and very weakly contrasted lamina strands between the NPCs. The average spacing is 1,670 ± 60 Å. (*c*) A nuclear envelope from *Xenopus* is shown. The background is filled with roughly triangular particles similar to large ribosomal subunits (57). (*Inset*) An oblique view of an NPC ejected from a membrane fold at the instant of freezing. The three-ringed architecture of the NPC is apparent. Bar, 2,400 Å.

~200 particles. Representative averages of membrane-associated NPCs from *Necturus* and *Xenopus* are shown in Fig. 10, *a* and *b*. The putative position of the membrane border (Fig. 10, *B*) and the radial spokes are consistent features of all the averages. As with the detergent-extracted NPCs, the radial arms are mirror symmetric.

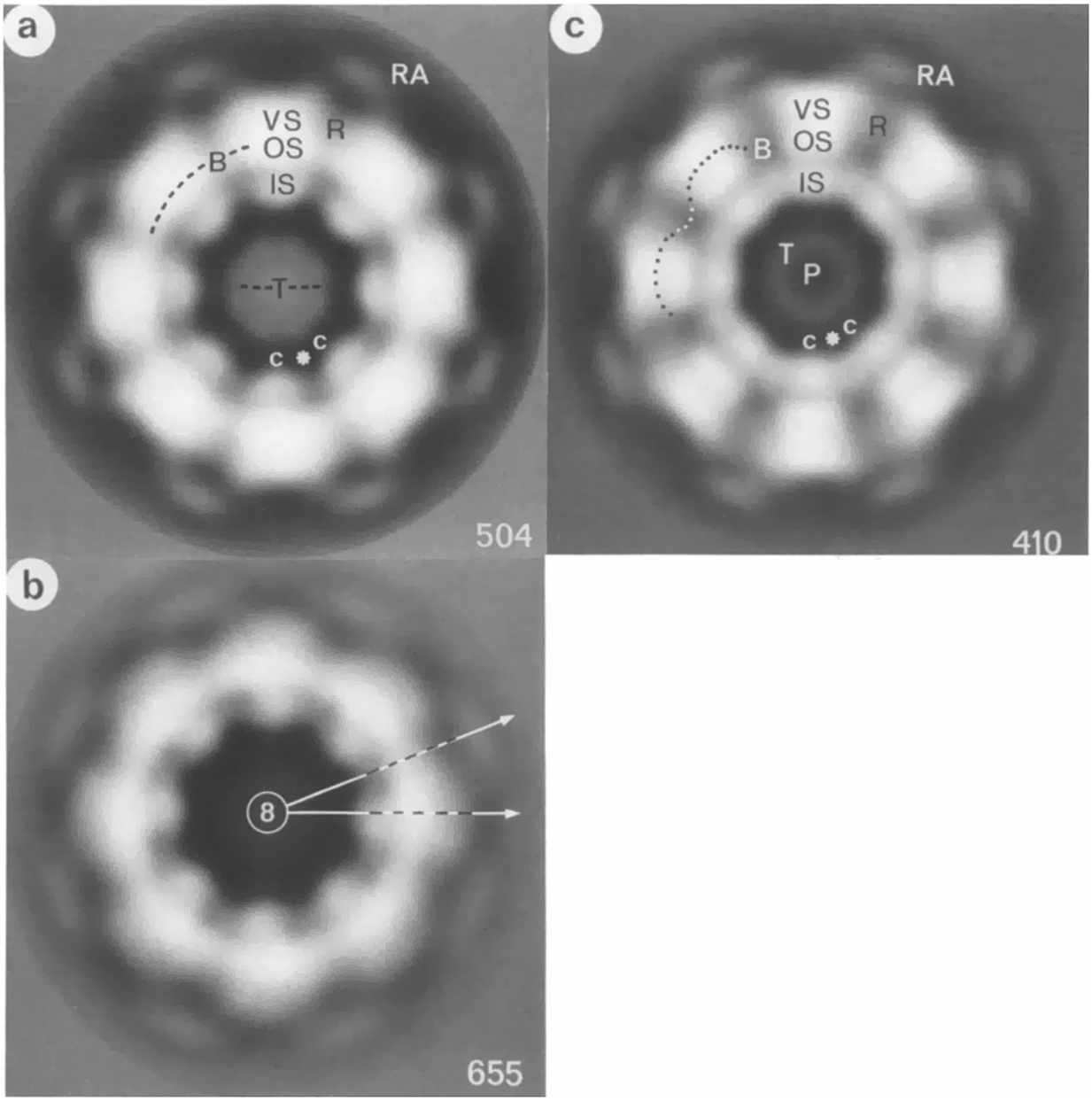

Figure 10. (*a*) A projection map of membrane-associated NPCs from *Necturus* (n = 504) in which the basic structural domains of the detergent-extracted NPCs are discernible and include the inner spoke domain (*IS*), the outer spoke domain (*OS*), the vertical supports (*VS*), the coaxial rings (*R*), and the radial arms (*RA*). In addition, the position of the membrane border (*dashed line*) can be observed as a bright ring of density which connects the spokes and appears to abut against the outer spoke domains. The centrally located transporter (*T*) is smeared out in these reconstructions. The white asterisk indicates a low density region between the framework of the pore complex and the transporter where passive diffusion of small molecules through the assembly may occur. A weak connecting density between the transporter and the spokes is observed reproducibly in most averages (*c*) at a lower cutoff. (*b*) Map of membrane-associated NPCs from *Xenopus* nuclei devoid of cytoplasmic particles. The position of the two approximate twofold axes are indicated by arrowed lines. (*c*) Averaged projection map of detergent-extracted NPCs (n = 410), with domains labeled as in *a* is shown for comparison. A possible profile of the encircling nuclear envelope is shown as a sinusoidal string of dots.

Features of the pore complex visualized in detergent-extracted NPCs were also observed in membrane-associated NPCs (see Fig. 10, *a* and *c*) and include the inner spoke domains (Fig. 10, *IS*), the outer spoke domains (Fig. 10, *OS*), the vertical supports (Fig. 10, *VS*), and the coaxial rings (Fig. 10, *R*). However, the membrane-associated NPCs have a handedness in contradistinction to detergent-extracted NPCs, and are always right-handed when viewed from the cytoplasm. The handedness is manifested in a radial slewing of the inner spoke domains and also in the density peaks which correspond to the juxtaposition of the outer spoke domains (Fig. 10, *OS*) with the membrane border. This latter asymmetric feature is masked in images photographed at the cutoff levels used in Fig. 10 to show the radial arms. The true

symmetry of the group averages of the membrane-associated NPCs in vitro is therefore eight rather than the more symmetrical 822. Furthermore, the central density associated with the NPC transporter (3) is variable in these maps, possibly as the result of the superposition of many different central motifs in the global averages.

Averages of membrane-associated NPCs from *Xenopus* were more consistent than those from *Necturus*, possibly due to similar ionic conditions during specimen freezing as the result of the smaller size of the nuclei. The average map from *Xenopus* (see Fig. 10 *b*) was obtained from specimens clearly devoid of large peripheral particles and therefore may represent the structure of the undecorated NPC. Many of the reconstructions from *Necturus* were qualitatively similar (data not shown). Differences in the two averages in Fig. 10, *a* and *b*, are primarily limited to the region labeled *VS* and may reflect perturbations of the assembly as the result of osmotic swelling during isolation of the nuclei. The magnitude of the density changes would seem to preclude the differential association of cytoplasmic particles as a principal source of the observed differences. As the result of these observations, it appears that membrane-associated NPCs in vitro are intrinsically asymmetric, possibly as the result of a conformational nonequivalence of their two halves resulting from interactions with the lamina and the nuclear envelope during isolation.

Discussion

NPC–Lamina Interactions

The nuclear lamina has been postulated to play a fundamental role in the organization of the nucleus. The lamina appears to serve as an architectural framework for the double nuclear envelope (26) and may serve as an anchoring site for interphase chromosomes (26, 36). Furthermore, the lamina may play a dynamic role in nuclear disassembly and assembly during mitosis (24, 25) because lamin association can be regulated by phosphorylation and dephosphorylation (27) and the lamina is located in a favorable position to mediate attachment of nuclear envelope vesicles onto daughter chromosomes in telophase (44, 51). Recently, it has become apparent that the lamins share many physical and structural characteristics in common with the intermediate filaments (2, 20, 38). It seems, therefore, that the physiological roles of the lamina arise from multivalent interactions with the nuclear envelope, nuclear pores, chromatin, and itself.

In this report, I have shown that the basic orthogonal lattice described for the lamina in *Xenopus* oocyte nuclei (2) also occurs in *Necturus*. However, the crossover spacings of the meshwork fall into two distinct classes. The first class appears to be responsible for the segregation of NPCs into the observed square arrays which occur in the nuclear envelope of *Necturus* with reasonably high frequency. Measured values for this repeat are probably more accurate when obtained from images of membrane-associated NPCs (Fig. 9 *b*; 1,670 ± 60 Å). Unusually close-packed arrays may possess a lattice repeat of 1,530 ± 40 Å (see Fig. 9 *a*), which probably represents the tightest possible packing of NPCs without interdigitation of their radial arms. The second class has a larger and more variable crossover repeat of ~3,000–4,000 Å. The reason for the existence of the two types of packing is unknown, but may be related to the large scale segregation of NPCs into areas of square and hexagonal packing which coexist in *Necturus* nuclei. Alternatively, lamin networks with the 3,000–4,000-Å crossover spacing may represent an intermediate in the assembly of the smaller class of lattices.

Although the role of the lamina in anchoring the NPCs has long been known (1), the precise manner in which this occurs has not been determined. Indirect evidence for the role of an as yet unidentified protein or lamin domain which mediates attachment of the NPCs to the lamina by way of the thin nucleoplasmic coaxial rings of the NPCs is as follows. First, the NPCs tend to pack within the confines of the smaller lamin network in *Necturus*. Second, disassembly of the NPCs often results in the nucleoplasmic ring being left embedded in the lamina. Third, NPCs in detergent-extracted and spread nuclei occasionally flip over resulting in edge-on views while still apparently attached to the lamina. Fourth, averages of detergent-extracted NPCs reveal a departure from strict 822 symmetry which could arise from NPC attachment to the lamina. The data on the arrangement of the *Necturus* oocyte lamina indicates that an ordered arrangement of the lamina may be a more general feature of nuclei. However, it is apparent that the lamina lattice is not necessarily restricted to the fundamental 520-Å repeat of the lamin family observed in *Xenopus* (2). Different cell types may possess ordered lamin networks with crossovers which are multiples of the 520-Å repeat as may be the case in nuclei from root tip cells of *Selaginella kraussima* (55).

A Modular Model of the NPC

The NPC is the communications gateway between the nucleus and the cytoplasmic machinery of the cell. An understanding of the pivotal role of the NPC in nucleocytoplasmic transport will necessitate solving the three-dimensional structure of the assembly, possibly in different transport-related configurations. The first step in this direction requires the implementation of a method to routinely obtain well preserved specimens for analysis. Nuclei from amphibian oocytes are preferred specimens for structural and functional analyses of the NPC as the result of their amenability to microdissection and the unusually high density of NPCs achieved in their nuclear envelopes. However, the ability to obtain reproducible and meaningful structural data, both in projection and in three dimensions, has been hampered by the inherent lability of this specimen although informative images have been obtained previously in negative stain (5, 17, 40, 58). Preparation of well preserved NPCs in amorphous ice should allow a more detailed structural analysis of the complex under conditions more closely approximating the native environment.

A modular model of NPC architecture based on a colinear alignment of three rings (as opposed to annuli of discrete subunits) was first described by Unwin and Milligan (40, 58). They demonstrated that the NPC is constructed from a central spoke assembly, presumably containing 16 spoke subunits, which is attached top and bottom to the coaxial nucleoplasmic and cytoplasmic rings at the outer surfaces of the membranes of the nuclear envelope. Further evidence for the existence of these separate components has been obtained using negative staining (5), heavy metal shadowing (5, 54), and embedding in amorphous ice (this work). A perspective

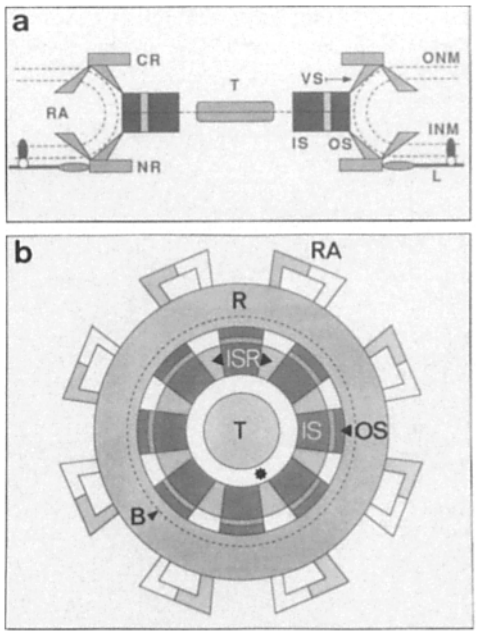

Figure 11. A revised model of the NPC proper, excluding details of the central transporter, is presented based on this work and thin sections (49). (*a*) Model of the detergent-extracted NPC presented in central cross section. The major structural domains are indicated including the inner spokes (*IS*), outer spokes (*OS*), vertical supports (*VS*), cytoplasmic and nucleoplasmic coaxial rings (*CR* and *NR*) and the radial arms (*RA*). The exact attachment site of the radial arms to the NPC along the vertical axis is not known. However, the radial arms project out past the membrane border in projection to radii of 720–750 Å. Attachment to the vertical supports near the membrane surfaces would minimize the size of these structures needed to project outwards this distance. The position of the observed weak density corresponding to the transporter is also indicated (*T*) and the lamina is shown schematically (*L*). The entities responsible for attachment of the lamina to the NPC and the inner nuclear membrane are unknown (but see reference 50). (*b*) A model of detergent-extracted NPCs viewed en face is shown as a pseudo projection. The major domains are again labeled as above and the maximum radius of the membrane border is also indicated (the dashed circle [*B*]). The asterisk indicates positions where passive exchange of small molecules may occur. The features observed in this study including the radial arms, the inner spoke ring, and the division between the inner and outer spoke domains are shown. The precise structure of the central channel assembly (*T*) is not known; hence, the central pore is not shown in this model.

drawing summarizing the triple ring model of the NPC in which the radial arms and lamina have been omitted and the size of the other components has been reduced for clarity is presented in Fig. 1. In this report, I have verified and extended this model of NPC architecture by visualizing new structural details of specimens in amorphous ice using quantitative single particle averaging. A model of the NPC incorporating these data is shown in Fig. 11, *a* and *b*, in central cross section and en face. Averages of edge-on views clearly indicate the presence of two apposed rings packed on either side of the central spokes. In addition, the rings appear to be rather complicated assemblies composed of elongated subunits comprised of at least four domains (not shown in the model) and maps of detergent-extracted NPCs have allowed direct visualization of the coaxial rings superposed on the central spoke assembly. In projection, the radial spokes have been resolved into three distinct domains including: (*a*) the inner spokes which are connected circumferentially to form an inner spoke ring (Fig. 11, *ISR*); (*b*) the outer spoke domains (Fig. 11, *OS*), which abut against the membrane border (Fig. 11, *a* and *b*, *dashed lines*) near the midline of the nuclear envelope; and (*c*) the vertical supports (Fig. 11, *VS*) which connect the central spokes to the nucleoplasmic and cytoplasmic coaxial rings (Fig. 11). Observations of partially disassembled NPCs both en face and edge-on, indicate that the coaxial rings are probably involved in holding the assembly together as postulated previously (40). In addition, direct evidence for the existence of an inner spoke ring was obtained in detergent-extracted NPCs.

Membrane Position and Anchoring of the NPC

The major role of the NPC in the cell is to mediate diffusion and transport of various molecules between the cytoplasmic and nuclear compartments. To this end, the NPC must maintain the incompletely fused state of the nuclear envelope and interactions between the NPC and the nuclear membranes play a crucial role in this process. A comparison between maps of membrane-associated and detergent-extracted NPCs is presented in Fig. 10, *a* and *c*. Although there are clear similarities between the two structures, there are also differences which presumably reflect NPC–membrane interactions. The first difference concerns the weaker density of the inner spoke ring in membrane-associated NPCs. Furthermore, the inner spoke domains (Fig. 10, *a* and *c*, *IS*) appear to lie off center of the in-plane twofold axes (see Fig. 10 *b*). A full understanding of these differences must await a three-dimensional analysis. The second obvious difference concerns the regions labeled *B* in the two forms. The average of the membrane-associated NPCs appears to have an extra ring of superposed density between radii of 360–470 Å. The phospholipid headgroups of the nuclear membranes are expected to contribute to the unstained image (23, 56); therefore, this additional density may represent the average location of the nuclear envelope as it passes around the periphery of the NPC as observed in thin sections (6, 18, 49) and in negatively stained nuclear envelopes from *Xenopus* denuded of their NPCs (58). Interestingly, the profile of the membrane may not be strictly circular but may conform to the local contours of the NPC. The reasoning for this is as follows. The density in region *B* (Fig. 10, *a* and *b*) is located between the spokes at similar radii as the outer spoke domain (Fig. 10, *OS*; see Table II). However, the *OS* domain is located at the level of the fused inner and outer nuclear membranes based on thin sections (6, 18, 49) and the edge-on reconstruction of detergent-extracted NPCs. The outer density in the spokes in Fig. 5 *a* is weaker (as expected in a cylindrically averaged structure), but extends fully to a radius of 470 Å consistent with the boundary between the *OS* and *VS* domains. Therefore, the radial displacement of the membrane appears to be ~100 Å over a 45° arc when viewed in projection. This would require that the profile of the encircling nuclear envelope have a modest eightfold sinusoidal variation which matches the local positions of components of the NPC (see Fig. 10 *c*). A similar plasticity of the Sindbis viral membrane has been shown recently in which the membrane forms an icosahedral-shaped shell sandwiched between the outer spike proteins and the inner (T = 3) capsid (23).

The NPCs appear to be anchored to the nuclear envelope in at least two ways. First, the NPCs are attached to the lamina (1), presumably by their nucleoplasmic coaxial rings. However, the identity of the component which tethers the lamina to the nuclear envelope is not known, but may correspond to a class of integral membrane proteins found only in the inner nuclear membrane which cross-react with the monoclonal antibody RL13 (50). Second, the radial arms (see Fig. 10, *a* and *c*) appear to be candidates for anchoring the NPCs to the nuclear envelope, possibly by spanning the nuclear membranes into the perinuclear space. Gerace and co-workers (28) have previously identified a transmembrane glycoprotein, gp-190, which binds both Con A and lentil lectins and remains with the NPC–lamina fraction after detergent extraction in low salt (as the radial arms behave in this work). Based on the abundance of the protein and immunolocalization studies using thin sections, they postulated that gp-190 might serve as an anchor for the NPC. Labeling studies are in progress to determine the nature of the radial arms; however, preliminary data suggest that Con A–gold is bound exclusively at a radius consistent with the radial arms in detergent-extracted NPCs but not in intact membranes. Therefore, the radial arms are shown in Fig. 11 *a* as protruding into the perinuclear space rather than extending along the membrane surface. A three-dimensional analysis will be required to unambiguously position this feature.

Confidence in the validity of the observed radial arm features can be attributed to four observations: (*a*) they are reproducible and occur in all 25 averages calculated in this study; (*b*) the radial arms are mirror symmetric within the limits of the data, implying that they originate from both halves of the NPC, whereas the observed interpore fibrils in *Xenopus* are cytoplasmic (54); (*c*) their existence is implied from a packing analysis of detergent-extracted NPC arrays (see below); and (*d*) eightfold averages of individual NPCs also demonstrate the radial arm motif, while the original images possess no single features which could spuriously give rise to the radial arms after symmetry averaging. The radial arms are visualized in the maps as the result of averaging over many repeats containing a weak signal, analogous to what occurs in crystallographic analysis. Furthermore, images of negatively stained square (58) and hexagonal (40) arrays of NPCs have been obtained previously and the measured interpore complex distance in these specimens is ~1,400 Å. This value is consistent with the effective diameter of the detergent-extracted NPCs determined from averages of frozen hydrated specimens, allowing for specimen shrinkage during negative staining. The radial arms appear to be present in close-packed NPCs but are not readily visualized by negative stain without extensive averaging. In addition, both square and hexagonal arrays of NPCs can be satisfactorily modeled using NPCs with radial arms: square packing mimics the two-dimensional plane group p422 with direct radial arm-to-radial arm contacts; while the hexagonally arrayed NPCs tend to pack as dimers on a p2 lattice with a lattice angle close to 120°.

Conclusions

In summary, the triple ring model of NPC architecture proposed by Unwin and Milligan (40, 58) is in good agreement with the projection structures of the detergent-extracted NPCs observed edge-on and en face in amorphous ice. A modular construction of the complex is obviously an important feature as the NPC is disassembled and reassembled during each mitotic cycle in many eukaryotic cells (45). The high degree of 822 symmetry displayed by detergent-extracted NPCs implies that the framework of this organelle is constructed of two equivalent or nearly equivalent halves; hence, the central spoke assembly must be comprised of 16 morphological units. The observed asymmetry of membrane-associated NPCs in the best preserved specimens obtained to date may have consequences for nucleocytoplasmic transport by affecting the environment of the central channel. Alternatively, the observed asymmetry may reflect osmotically induced rearrangements incurred during isolation of the nuclei. As shown in this work, a central channel-like feature is evident in micrographs of the best preserved detergent-extracted NPCs. Furthermore, this feature can be selectively labeled with nucleoplasmin, WGA, and a monoclonal against members of the O-linked *N*-acetylglucosamine family of nucleoporins (3). Three-dimensional analyses of representative NPCs with and without membranes are now needed, in conjunction with a further analysis of the variable structure of the central channel.

This work has greatly benefited from the criticisms of P. N. T. Unwin and M. Stewart. In addition I wish to thank my colleagues in the Department of Cell Biology at Stanford University Medical School for their support during the course of this work; P. N. T. Unwin and R. A. Milligan for making available images of negatively stained rings and NPCs for analysis; and M. Radermacher and J. Frank for their contributions in implementing the SPIDER software.

This work was supported by the National Institutes of Health (R23-AM34164-02).

Received for publication 26 January 1989 and in revised form 1 June 1989.

References

1. Aaronson, R. P., and G. Blobel. 1975. Isolation of nuclear pore complexes in association with a lamina. *Proc. Natl. Acad. Sci. USA.* 72:1007–1011.
2. Aebi, U., J. Cohn, L. Buhle, and L. Gerace. 1986. The nuclear lamina is a meshwork of intermediate-type filaments. *Nature (Lond.).* 323:560–564.
3. Akey, C. W., and D. S. Goldfarb. 1989. Protein import through the nuclear pore complex is a multistep process. *J. Cell Biol.* 109:971–982.
4. Bonner, W. M. 1975. Protein migration into nuclei. I. Frog nuclei in vivo accumulate microinjected histones, allow entry to small proteins, and exclude large proteins. *J. Cell Biol.* 64:421–430.
5. Buhle, L., and U. Aebi. 1985. Correlation of surface topography of metal shadowed specimens with their negatively stained reconstructions. *Ultramicroscopy.* 16:436–450.
6. Daniels, E. W., J. M. McNiff, and D. R. Ekberg. 1969. Nucleopores of the giant amoeba, *Pelomyxa carolinensis. Z. Zellforsch. Mikrosk. Anat.* 98:357–368.
7. Davey, J., N. J. Dimnock, and A. Colman. 1985. Identification of the sequence responsible for the nuclear accumulation of the influenza virus nucleoprotein in *Xenopus* oocytes. *Cell.* 40:667–675.
8. Davis, L. I., and G. Blobel. 1986. Identification and characterization of a nuclear pore complex protein. *Cell.* 45:699–709.
9. Davis, L. I., and G. Blobel. 1987. Nuclear pore complex contains a family of glycoproteins that includes p62: glycosylation through a previously unidentified cellular pathway. *Proc. Natl. Acad. Sci. USA.* 84:7552–7556.
10. DeRobertis, E. M., R. E. Longthorne, and J. B. Gurdon. 1978. The intracellular migration of nuclear proteins in *Xenopus* oocytes. *Nature (Lond.).* 272:254–256.
11. Dingwall, C., and R. A. Laskey. 1986. Protein import into the cell nucleus. *Annu. Rev. Cell Biol.* 2:367–390.
12. Dingwall, C., S. V. Sharnick, and R. A. Laskey. 1982. A polypeptide domain that specifies migration of nucleoplasmin into the nucleus. *Cell.* 30:449–458.
13. Dubochet, J., M. Groom, and S. Mueller-Neuteboom. 1982. The mounting of macromolecules for electron microscopy with particular reference to surface phenomena and the treatment of support films by glow discharge. *Adv. Opt. Electron Microsc.* 8:107–135.

14. Dubochet, J., J. Lepault, R. Freeman, J. A. Berriman, and J. C. Homo. 1982. Electron microscopy of frozen water and aqueous solutions. *J. Microsc. (Paris).* 128:219–237.
15. Dworetzky, S. J., and C. M. Feldherr. 1988. Translocation of RNA-coated gold particles through the nuclear pores of oocytes. *J. Cell Biol.* 106: 575–584.
16. Erickson, H. P., and A. Klug. 1971. Measurement and compensation of defocusing and aberrations by Fourier processing of electron micrographs. *Philos. Trans. R. Soc. Lond. B. Biol. Sci.* 261:105–118.
17. Faberge, A. C. 1973. Direct demonstration of eightfold symmetry in nuclear pores. *Z. Zellforsch Mikrosk. Anat.* 136:183–190.
18. Feldherr, C. M., E. Kallenback, and N. Schultz. 1984. Movement of a karyophillic protein through the nuclear pores of oocytes. *J. Cell Biol.* 99:2216–2222.
19. Finlay, D. R., D. D. Newmeyer, T. M. Price, and D. J. Forbes. 1987. Inhibition of in vitro nuclear transport by a lectin that binds to nuclear pores. *J. Cell Biol.* 104:189–200.
20. Fisher, D., N. Chaudhary, and G. Blobel. 1986. cDNA sequencing of nuclear lamins A and C reveals primary and secondary structural homology to intermediate filaments. *Proc. Natl. Acad. Sci. USA.* 83:6450–6454.
21. Frank. J., B. Shimkin, and H. Dowse. 1981. SPIDER-A modular software system for electron image processing. *Ultramicroscopy.* 6:343–358.
22. Franke, W. W. 1974. Structure, biochemistry and functions of the nuclear envelope. *Int. Rev. Cytol.* 4(Suppl.):71–236.
23. Fuller, S. D. 1987. The T=4 envelope of Sindbis virus is organized by interactions with a T=3 capsid. *Cell.* 48:923–934.
24. Gerace, L. 1986. Nuclear lamina and organization of the nuclear architecture. *Trends Biochem. Sci.* 11:443–446.
25. Gerace, L., and G. Blobel. 1982. Nuclear lamina and the structural organization of the nuclear envelope. *Cold Spring Harbor Symp. Quant. Biol.* 46:967–978.
26. Gerace, L., A. Blum, and G. Blobel. 1978. Immunocytochemical localization of the major polypeptides of the nuclear pore complex. *J. Cell Biol.* 79:546–566.
27. Gerace, L., C. Comeau, and M. J. Benson. 1984. Organization and modulation of nuclear lamina structure. *J. Cell Sci. Suppl.* 1:137–160.
28. Gerace, L., Y. Ottaviano, and C. Kondor-Koch. 1982. Identification of a major polypeptide of the nuclear pore complex. *J. Cell Biol.* 95:826–837.
29. Goldfarb, D. S., J. Gariepy, G. Schoolnik, and R. D. Kornberg. 1986. Synthetic peptides as nuclear localization signals. *Nature (Lond.).* 322:641–644.
30. Gurdon, J. B. 1976. Injected nuclei in oocytes: fate, enlargement and chromatin dispersal. *J. Embryol. Exp. Morphol.* 36:523–540.
31. Hoeijmakers, J. H. J., J. H. N. Schel, and F. Wanka. 1974. Structure of the nuclear pore complex in mammalian cells. Two annular components. *Exp. Cell Res.* 87:197–206.
32. Homo, J. C., F. Booy, P. Labouesse, J. Lepault, and J. Dubochet. 1984. Improved anticontaminator for cryoelectron microscopy with Philips EM 400. *J. Microsc. (Paris).* 136:337–340.
33. Kalderon, D., B. C. Roberts, W. D. Richardson, and A. E. Smith. 1984. A short amino acid sequence able to specify nuclear location. *Cell.* 39:499–509.
34. Deleted in proof.
35. Krohne, G., W. Franke, and U. Scheer. 1978. The major polypeptides of the nuclear pore complex. *Exp. Cell Res.* 116:85–102.
36. Lebkowski, J., and U. Laemmli. 1982. Non-histone proteins and long range organization of HeLa interphase DNA. *J. Mol. Biol.* 156:325–344.
37. Maul, G. 1977. The nuclear and cytoplasmic pore complex: structure, dynamics, distribution and evolution. *Int. Rev. Cytol.* 6(Suppl.):75–186.
38. McKeon, F., M. Kirshner, and D. Caput. 1986. Homologies in both primary and secondary structure between nuclear envelope and intermediate filament proteins. *Nature (Lond.).* 319:463–468.
39. Melton, D. A., E. M. DeRobertis, and R. Cortese. 1980. Order and intracellular location of the events involved in maturation of a spliced t-RNA. *Nature (Lond.).* 284:143–148.
40. Milligan, R. A. 1986. A structural model for the nuclear pore complex. *In* Nucleocytoplasmic Transport. R. Peters and M. Trendelenburg, editors. Springer-Verlag, New York. 113–122.
41. Milligan, R. A., A. Brisson, and P. N. T. Unwin. 1984. Molecular structure determination of crystalline specimens in frozen aqueous solutions. *Ultramicroscopy.* 13:1–10.
42. Newmeyer, D. D., D. R. Finlay, and D. J. Forbes. 1986. In vitro transport of a fluorescent nuclear protein and exclusion of nonnuclear proteins. *J. Cell Biol.* 103:2091–2102.
43. Newmeyer, D. D., J. M. Lucocq, T. R. Burglin, and E. M. DeRobertis. 1986. Assembly in vitro of nuclei active in nuclear protein transport: ATP is required for nucleoplasmic accumulation. *EMBO (Eur. Mol. Biol. Organ.) J.* 5:501–510.
44. Newport, J. 1987. Nuclear reconstitution in vitro: stages of assembly around protein-free DNA. *Cell.* 48:205–217.
45. Newport, J. W., and D. J. Forbes. 1987. The nucleus: structure, function and dynamics. *Annu. Rev. Biochem.* 56:535–565.
46. Paine, P. L., L. C. Moore, and S. B. Horowitz. 1975. Nuclear envelope permeability. *Nature (Lond.).* 254:109–114.
47. Peters, R. 1984. Nucleocytoplasmic flux and intracellular mobility in single hepatocytes measured by fluorescence microphotolysis. *EMBO (Eur. Mol. Biol. Organ.) J.* 3:1831–1836.
48. Richardson, W. D., B. C. Roberts, and A. E. Smith. 1986. Nuclear location signals in polyoma large-T. *Cell.* 44:77–85.
49. Roberts, K., and D. H. Northcote. 1970. Structure of the nuclear pore in higher plants. *Nature (Lond.).* 228:385–386.
50. Senior, A., and L. Gerace. 1988. Integral membrane proteins specific to the inner nuclear membrane and associated with the nuclear lamina. *J. Cell Biol.* 107:2029–2036.
51. Sheehan, M. A., A. D. Mills, A. M. Sleeman, R. A. Laskey, and J. J. Blow. 1988. Steps in the assembly of replication-competent nuclei in a cell-free system from *Xenopus* eggs. *J. Cell Biol.* 106:1–12.
52. Snow, C. M., A. Senior, and L. Gerace. 1987. Monoclonal antibodies identify a group of nuclear pore complex glycoproteins. *J. Cell Biol.* 104:1143–1156.
53. Stevens, B. J., and H. Swift. 1966. RNA transport from nucleus to cytoplasm in *Chironomus* salivary glands. *J. Cell Biol.* 31:55–77.
54. Stewart, M., and S. Whytock. 1988. The structure and interactions of components of nuclear envelopes from *Xenopus* oocyte germinal vesicles observed by heavy metal shadowing. *J. Cell Sci.* 90:409–423.
55. Thair, B. W., and A. B. Wardrop. 1971. The structure and arrangement of nuclear pores in plant cells. *Planta (Berl.).* 100:1–17.
56. Toyoshima, C., and P. N. T. Unwin. 1988. Ion channel of acetylcholine receptor reconstructed from images of postsynaptic membranes. *Nature (Lond.).* 336:247–250.
57. Toyoshima, C., and P. N. T. Unwin. 1988. Contrast transfer for frozen hydrated specimens: determination from pairs of defocused images. *Ultramicroscopy.* 25:279–292.
58. Unwin, P. N. T., and R. A. Milligan. 1982. A large particle associated with the perimeter of the nuclear pore complex. *J. Cell Biol.* 93:63–75.
59. Virtanen, I., and J. Wartiovaara. 1978. Distribution of lectin binding sites on rat liver cell nuclei: comparison of fluorescein and ferritin labeling methods. *Cell. Mol. Biol.* 23:73–79.
60. Wickens, M. P., and J. B. Gurdon. 1983. Post-translational processing of simian virus 40 late transcripts in injected frog oocytes. *J. Mol. Biol.* 163:1–26.
61. Zasloff, M. 1983. t-RNA transport from the nucleus in a eukaryotic cell: a carrier mediated translocation process. *Proc. Natl. Acad. Sci. USA.* 80:6436–6440.